Int. J. Heat Mass Transfer. Vol. 25, No. 4 pp. 499–511, 1982
Printed in Great Britain

0017–9310/82/040499–13 $03.00/0

NATURAL CONVECTION IN A VERTICAL CHANNEL WITH OPPOSING BUOYANCY FORCES

T. S. LEE, P. G. PARIKH, A. ACRIVOS and D. BERSHADER
Stanford University, Stanford, CA 94305, U.S.A.

(*Received* 12 *January* 1981 *and in revised form* 18 *September* 1981)

Abstract—Free convection in a vertical channel within which the buoyancy force reverses its sign has been studied experimentally and theoretically. The experimental system consisted of a channel formed between two vertical plates, one porous and the other solid. Both plates were maintained at uniform surface temperatures, higher than the ambient, while a heavy gas (CO_2) was transpired into the channel through the porous plate. The temperature and CO_2 concentration fields in the channel were measured by combined use of a thermocouple probe and Mach–Zehnder interferometry.

The temperature and concentration fields were also determined via a finite difference solution of the time dependent boundary layer equations. As the time dependent equations are parabolic in time, the solution may be stepped forward in time using centered finite differences for spatial derivatives until a steady state solution is reached. A finite difference scheme may thus be constructed which is stable regardless of the sign of the streamwise velocity component.

The solutions thus obtained reveal many interesting features of this complex flow, including the effects of opposing buoyancy forces on the axial velocity profiles. Measured profiles of temperature and concentration showed close agreement with the theoretical predictions.

NOMENCLATURE

b, channel width;
C_a, specific heat of air;
C_g, specific heat of injected gas,
C_p, specific heat of mixture;
$\mathscr{D}$, diffusion coefficient;
g, gravitational acceleration;
G_{diff}, diffusional flux of injected species;
Gr_T, $= g(T_{w,2} - T_\infty)b^4/l\nu_\infty^2 T_\infty$, Grashof number;
Gr_m, $= g(1 - \hat{M}_a/\hat{M}_g)b^4/l\nu_\infty^2$, Grashof number;
k, thermal conductivity of mixture;
K_a, Dale–Gladstone constant for air;
l, channel height;
m, mass fraction of injected species;
m_T, mass fraction of species in injected mixture;
$\dot{m}_o''$, mass flux at the porous surface;
$\hat{M}_a$, molecular weight of air;
$\hat{M}_g$, molecular weight of injected species;
n_a, refractive index of air;
n_{CO_2}, refractive index of CO_2;
p, pressure;
Pr, Prandtl number;
R_t, $= (T_{w,1} - T_\infty)/(T_{w,2} - T_\infty)$, non-dimensional wall temperature ratio;
S, fringe shift;
Sc, Schmidt number;
t, time;
T, temperature;
T_∞, ambient temperature;
$\bar{T}$, average of wall temperatures $\frac{1}{2}(T_{w,1} + T_{w,2})$;
$T_{w,1}$, temperature of the porous plate;
$T_{w,2}$, temperature of heated plate;
u, streamwise velocity component;
U, $= b^2 u/l\nu_\infty Gr_m$, non-dimensional streamwise velocity;
v, velocity component normal to wall;
v_T, $= \dot{m}_o''/\rho_T$, injected gas velocity;
V, $= bv/\nu_\infty$, non-dimensional velocity component normal to the wall;
W, $= m/m_T$, normalized CO_2 concentration in the mixture;
x, streamwise coordinate;
y, coordinate normal to the walls;
X, $= x/l/Gr_m$; non-dimensional streamwise coordinate;
Y, $= y/b$, non-dimensional normal coordinate.

Greek letters

ρ, mixture density;
μ, mixture viscosity;
τ, $= tb^2/\nu_\infty$, non-dimensional time;
ν, mixture kinematic viscosity;
θ, $= (T - T_\infty)/(T_{w,2} - T_\infty)$, non-dimensional temperature;
λ, wavelength or property ratio of subscripted property;
χ, mole fraction;
ϕ, $= T/T_\infty$, temperature ratio.

INTRODUCTION

THERE are several practical situations of free convection flow driven by opposing buoyancy forces. In many such cases, the net buoyancy force acting on a fluid element may reverse its direction within the flow field and may ultimately lead to the reversal in the

direction of the local fluid velocity. Examples may be found in certain chemical processes, where the evaporation or sublimation of heavy organic vapors from heated surfaces leads to a species concentration buoyancy force which opposes that due to thermal effects. A similar situation can arise in the free convective burning of a vertical cellulosic fuel surface where heavy, gaseous pyrolysis products transpire into a high temperature boundary layer. Simultaneous diffusion of heat and salinity in sea water also induces free convection currents driven by opposing buoyancy forces. Finally, the occurrence of a density extremum in water close to its freezing point gives rise to a buoyancy force reversal within the boundary layer close to the solid–fluid interface [1, 2].

A number of investigations, both analytical and experimental, of such combined (aiding or opposing) buoyancy flows have been reported, notably in the chemical engineering literature, and many of these were summarized by Gebhart and Pera [3]. The analytical approach in these earlier investigations has been limited to obtaining solutions either by integral methods or via similarity transformations of the boundary layer equations. As pointed out by [3], however, integral methods (which at best are only approximate) are inadequate for describing the complicated structure of flows with reversal, while, on the other hand, similarity solutions to the boundary layer equations can exist only under certain very specialized conditions.

For example, Adams and Lowell [4] attempted to construct similarity solutions for the problem of organic sublimation from heated vertical surface. The Schmidt number for the organic vapor diffusing in air was 2.5, while the Prandtl number for diffusion of heat through the mixture was approx. 0.7. Adams and Lowell found that similarity solutions existed only so long as the flow remained unidirectional. This problem was also considered by [3] over a range of Prandtl and Schmidt number values; they found that similarity solutions did in fact exist for certain combinations of Prandtl and Schmidt numbers even when flow reversal occurred within the boundary layer. Specifically, in a case involving opposing buoyancy forces with $Pr = 0.7$ and $Sc = 0.5$, the predicted self-similar velocity profile exhibited flow reversal in the outer region of the boundary layer. Similarly, for the case of $Pr = 0.7$ and $Sc = 5.0$, the predicted self-similar velocity profile indicated a flow reversal close to the wall.

Similarity solutions to the boundary layer equations were recently sought by Carey *et al.* [1] for the problem of natural convection in the vicinity of an ice surface in cold water. Calculations were carried out into the temperature range where the buoyancy force reversed its direction across the boundary layer. However, the numerical scheme would not converge over most of the temperature range where flow reversal was present.

The three studies mentioned above tacitly assumed the presence of a semi-infinite surface over which natural convection flows occur under the action of combined buoyancy forces. Clearly though, if the surface is of a finite length then the existence of flow reversal will cause the flow field to be influenced by the presence of a "trailing" edge, and such upstream influence will not be taken into account by any similarity solution (which, if it exists, is strictly valid only for a semi-infinite plate or near the leading edge of a surface of finite length).

To summarize, then, similarity solutions to the problem of natural convection past a (semi-infinite) vertical flat plate with opposing buoyancy forces have been found to exist only for a very small range of parameters leading to flow reversal. Even where such solutions have been determined via a numerical solution of the resulting ordinary differential equations, their applicability to problems involving plates of finite length appears questionable, as these solutions do not account for the upstream influence.

The applicability of similarity solutions to boundary layer equations with flow reversal was discussed in some detail by Klemp and Acrivos [5] with reference to the problem of boundary layer flow past a finite plate with a negative surface velocity. These authors found that, surprisingly, a similarity solution (for a semi-infinite plate length) exists only when the ratio of the speed of the plate surface to that of the free-stream is less than 0.3541, and that, furthermore, this similarity solution remains valid only in the immediate vicinity of the leading edge of a finite length plate as the critical speed ratio of 0.3541 is approached. The complete solution of the problem, applicable for all plate surface speeds and over the entire length of a finite plate, was obtained subsequently [6] by means of a novel computational scheme which solved the time dependent governing equations of the problem.

It is clear that the range of applicability of similarity solutions to problems involving natural convection flow in the vicinity of a *finite* vertical plate is rather limited when flow reversal occurs. A solution technique more advanced than any of those previously employed is needed to deal with such problems. In the present study, numerical solutions to the problem of natural convection between vertical parallel plates, including the effects of opposing buoyancy forces, have been obtained as steady state solutions of time dependent governing equations. The solution technique employed here is essentially the same as that of [6]. The advantage of using this transient method of solution is that the time dependent boundary layer equations are parabolic in time; therefore, they can be stepped forward in time using centered finite differences for spatial derivatives in x. Thus, a finite difference scheme may be constructed which is stable regardless of the sign of streamwise velocity component u.

The objectives of the present study were to establish a free convection flow field with a reversing buoyancy

force and to compare the experimental results with the finite difference solution of the corresponding governing equations.

In a previous study [7] an attempt was made to set up a stable, reversing buoyancy flow field in the vicinity of a heated, vertical porous plate by transpiring CO_2. However, as the Lewis number of CO_2 diffusing in air was close to unity, the species boundary layer had almost the same thickness as that of the thermal boundary layer. Consequently, the net buoyancy force distribution across the boundary layer was either unidirectional or very close to zero. In the latter case, the boundary layer was highly unstable and very difficult to study experimentally.

These difficulties were circumvented in the present experiments by placing a heated plate facing the transpiring porous plate, thereby forming a vertical channel between the two plates, as shown in Fig. 1. By this arrangement, the location of maximum thermal buoyancy force ($y = b$) was separated from the location of maximum species buoyancy force ($y = 0$). When a heavy gas (CO_2 in the present study) was transpired through the porous plate, a stable flow field, in which the net buoyancy force reversed its direction across the channel, could be established over a range of parameters.

The problem of developing free convection in a vertical channel with both walls heated and no transpiration has been studied extensively in many previous investigations [8–10]. However, the case of free convection in a channel with a reversing buoyancy force has received very little attention. A simple analysis to predict a "fully developed" natural convection flow between parallel planes with one wall heated and the other cooled was presented by Rohsenow and Choi [14]. In that analysis the temperature and velocity profiles were assumed to remain invariant along the streamwise direction, thereby reducing the mathematical system to ordinary differential equations. The solution to these equations led to a linear variation of the fluid temperature between the walls and a cubic velocity profile. Obviously, such a solution could possibly be valid at best only far away from the entrance and exit ends of a very long channel.

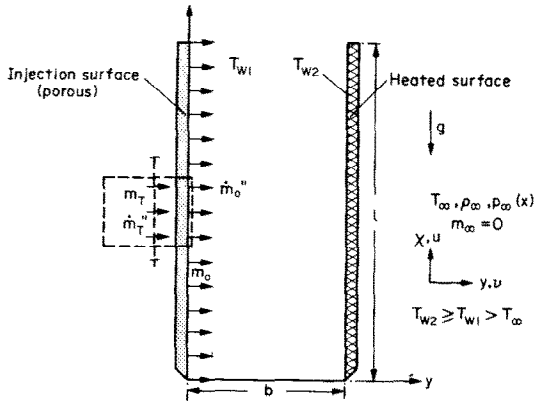

FIG. 1. Schematic diagram of the channel and coordinate system.

GOVERNING EQUATIONS AND SOLUTION TECHNIQUE

The time dependent, 2-dim. variable property equations are:

continuity

$$\frac{\partial \rho}{\partial t} + \frac{\partial(\rho u)}{\partial x} + \frac{\partial(\rho v)}{\partial y} = 0,$$

x-momentum

$$\rho\left(\frac{\partial u}{\partial t} + u\frac{\partial u}{\partial x} + v\frac{\partial u}{\partial y}\right) = -\rho g - \frac{\partial p}{\partial x} + \frac{\partial}{\partial y}\left(\mu\frac{\partial u}{\partial y}\right),$$

energy

$$\rho C_p\left(\frac{\partial T}{\partial t} + u\frac{\partial T}{\partial x} + v\frac{\partial T}{\partial y}\right) = \frac{\partial}{\partial y}\left(k\frac{\partial T}{\partial y}\right) - G_{diff}(C_g - C_a)\frac{\partial T}{\partial y},$$

species

$$\rho\left(\frac{\partial m}{\partial t} + u\frac{\partial m}{\partial x} + v\frac{\partial m}{\partial y}\right) = \frac{\partial}{\partial y}\left(\rho\mathscr{D}\frac{\partial m}{\partial y}\right),$$

where the usual boundary layer approximations have been invoked.

The use of boundary layer-type approximations is justified, provided the channel height is at least several times the channel width. In this "narrow channel" situation, the magnitude of the streamwise component of the velocity is large compared to that of the transverse component, while the gradients normal to the wall are large compared with those along the streamwise direction. These requirements may be violated locally within some regions in the flow field, as in the case with boundary layer equations near the leading edge of a stationary flat plate in uniform flow. However, away from these singular regions, a physically realistic solution can generally be obtained.

In the energy equation, the viscous dissipation pressure work and diffusion thermo terms are neglected. The body force per unit mass in the momentum equation is the gravitational acceleration g, directed in the negative x-direction, as shown in Fig. 1.

Now p is the pressure existing in the channel at an elevation x. We can define a pressure defect $p'(x)$ such that

$$p'(x) = p(x) - p_\infty(x),$$

where $p_\infty(x)$ is the ambient pressure, defined by

$$\frac{dp_\infty(x)}{dx} = -\rho_\infty g$$

hence

$$\frac{\partial p}{\partial x} = \frac{\partial p'}{\partial x} + \frac{dp_\infty}{dx} = \frac{\partial p'}{\partial x} - \rho_\infty g.$$

Substitution in the x-momentum equation yields:

x-momentum

$$\frac{\partial u}{\partial t}+u\frac{\partial u}{\partial x}+v\frac{\partial u}{\partial y}=-\frac{1}{\rho}\frac{\partial p'}{\partial x}+\frac{g(\rho_\infty-\rho)}{\rho}+\frac{1}{\rho}\frac{\partial}{\partial y}\left(\mu\frac{\partial u}{\partial y}\right). \quad (1)$$

The density field inside the channel is a function of both temperature and concentration. For small values of $(T-T_\infty)/T_\infty$, $(p-p_\infty)/p_\infty$, and m,

$$\frac{\rho_\infty-\rho}{\rho}=\frac{(T-T_\infty)}{T_\infty}+\left[\frac{\hat{M}_a}{\hat{M}_g}-1\right]m.$$

Hence, equation (1) becomes:

x-momentum

$$\frac{\partial u}{\partial t}+u\frac{\partial u}{\partial x}+v\frac{\partial u}{\partial y}=-\frac{1}{\rho}\frac{\partial p'}{\partial x}+\frac{g(T-T_\infty)}{T}+g\left[\frac{\hat{M}_a}{\hat{M}_g}-1\right]m+\frac{1}{\rho}\frac{\partial}{\partial y}\mu\frac{\partial u}{\partial y}. \quad (2)$$

The various dependent and independent variables appearing in the above relation will next be non-dimensionalized using the following groupings:

$$X=\frac{x}{lGr_m};\quad Y=\frac{y}{b};\quad \tau=\frac{tb^2}{\nu_\infty};$$

$$U=\frac{b^2u}{l\nu_\infty Gr_m};\quad V=\frac{bv}{\nu_\infty};\quad \bar{m}=\frac{m}{m_T};$$

$$\theta=\frac{T-T_\infty}{T_{w,2}-T_\infty};\quad \bar{\theta}=\frac{T-T_\infty}{\bar{T}-T_\infty}=\frac{R_t+1}{2}\theta;$$

$$V_T=\frac{bv_T}{\nu_\infty};\quad P=\frac{p'b^4}{\rho_\infty l^2\nu_\infty^2(Gr_m)^2}.$$

In the above definitions, a mass transfer Grashof number defined as

$$Gr_m=\frac{g\left(1-\frac{\hat{M}_a}{\hat{M}_g}\right)b^4}{l\nu_\infty^2}$$

has been introduced. Also, m_T is the mass concentration of CO_2 in the injected gas ($m_T=1$ in this study):

$$\bar{T}=\frac{1}{2}(T_{w,1}+T_{w,2}),$$

$$R_t=\frac{T_{w,1}-T_\infty}{T_{w,2}-T_\infty},$$

and

$$v_T=\frac{\dot{m}''}{\rho_T}.$$

Two Grashof numbers based on temperature differences may be defined:

$$\overline{Gr_T}=\frac{g(\bar{T}-T_\infty)b^4}{l\nu_\infty^2T_\infty}\quad\text{and}\quad Gr_T=\frac{g(T_{w,2}-T_\infty)b^4}{l\nu_\infty^2T_\infty}.$$

The governing equations may then be written in terms of non-dimensional variables, as follows:

continuity

$$\frac{\partial\lambda_\rho}{\partial t}+\frac{\partial(\lambda_\rho U)}{\partial X}+\frac{\partial(\lambda_\rho V)}{\partial Y}=0, \quad (3)$$

momentum

$$\frac{\partial U}{\partial\tau}+U\frac{\partial U}{\partial X}+V\frac{\partial U}{\partial Y}=-\frac{1}{\lambda_\rho}\frac{dP}{dX}+\frac{1}{\lambda_\rho}\lambda_\mu\frac{\partial U}{\partial Y}+\left(\bar{\theta}\frac{\overline{Gr_T}}{Gr_m}-\bar{m}\right), \quad (4)$$

energy

$$\frac{\partial\bar{\theta}}{\partial\tau}+U\frac{\partial\bar{\theta}}{\partial X}+V\frac{\partial\bar{\theta}}{\partial Y}=\frac{1}{Pr_\infty}\frac{1}{\lambda_\rho\lambda_{C_p}}\frac{\partial}{\partial Y}\left(\lambda_k\frac{\partial\bar{\theta}}{\partial Y}\right)+\frac{1}{Sc_\infty}\frac{\lambda_{\mathscr{D}}}{\lambda_{C_p}}\left(\frac{c_g}{c_a}-1\right)\frac{\partial\bar{\theta}}{\partial Y}\frac{\partial\bar{m}}{\partial Y}, \quad (5)$$

species

$$\frac{\partial\bar{m}}{\partial\tau}+U\frac{\partial\bar{m}}{\partial X}+V\frac{\partial\bar{m}}{\partial Y}=\frac{1}{Sc_\infty}\frac{1}{\lambda_\rho}\frac{\partial}{\partial Y}\left(\lambda_\rho\lambda_{\mathscr{D}}\frac{\partial\bar{m}}{\partial Y}\right). \quad (6)$$

The quantities λ appearing in the above equations are the ratios of variable properties normalized by their ambient value.

To complete the formulation of the problem, it is necessary to specify the initial and boundary conditions of this transient, 2-dim. problem.

The initial condition at time $\tau=0$ was chosen as the steady state solution of the channel flow problem with a uniform transpiration of CO_2 at the porous wall and both the walls at the ambient temperature T_∞. At time $\tau=0_+$, the appropriate boundary conditions for temperature are suddenly applied at the two walls and the subsequent evolution of the flow field is computed by means of a finite difference technique.

A separate finite difference program was used to compute the flow field at $\tau=0_-$. This program was, in principle, similar to the one employed by Bodia and Osterle [8], except that a more exact pressure condition was used at the channel entrance to account for the acceleration of fluid from zero ambient velocity to its value at the channel entrance plane. The same pressure condition at the channel entrance was employed in [9, 10] for an improved prediction. Thus the intial conditions at $\tau=0_-$ are:

$$U(X,Y)=\hat{U}(X,Y),$$

$$V(X,Y)=\hat{V}(X,Y),$$

$$\bar{m}(X,Y)=\hat{\bar{m}}(X,Y),\quad 0\le X\le\frac{1}{Gr_m},$$

$$P(X)=\hat{P}(X),$$

$$\bar{\theta}(X,Y)=0,$$

where $\hat{U}$, $\hat{V}$ etc. are solutions of the channel flow problem with transpiration of CO_2 and unheated walls. The details of the solution procedure for $\hat{U}$, $\hat{V}$ etc. are presented in [11].

The boundary conditions at the two walls remain unchanged with time for $\tau > 0_+$ for all dependent variables. In non-dimensional form, the boundary condition at the porous wall becomes

$$U = 0, \quad V = \frac{\lambda_{\rho,T}}{\lambda_{\rho,0}} V_T, \quad \bar{\theta} = R_t\left(\frac{1+R_t}{2}\right),$$

$$\bar{m}_o = 1 + \frac{\lambda_{\mathscr{D},o}}{Sc_o}\frac{1}{V_o}\frac{\partial \bar{m}}{\partial Y}\bigg|_{Y=0} \quad \text{at } Y = 0;\ 0 < X < \frac{1}{Gr_m}$$

and $\tau > 0_+$.

At the solid wall,

$$U = 0; \quad V = 0; \quad \bar{\theta} = \frac{1+R_t}{2}; \quad \frac{\partial \bar{m}}{\partial Y} = 0$$

$$\text{at } Y = 1, \quad 0 < X < \frac{1}{Gr_m}, \quad \tau > 0_+.$$

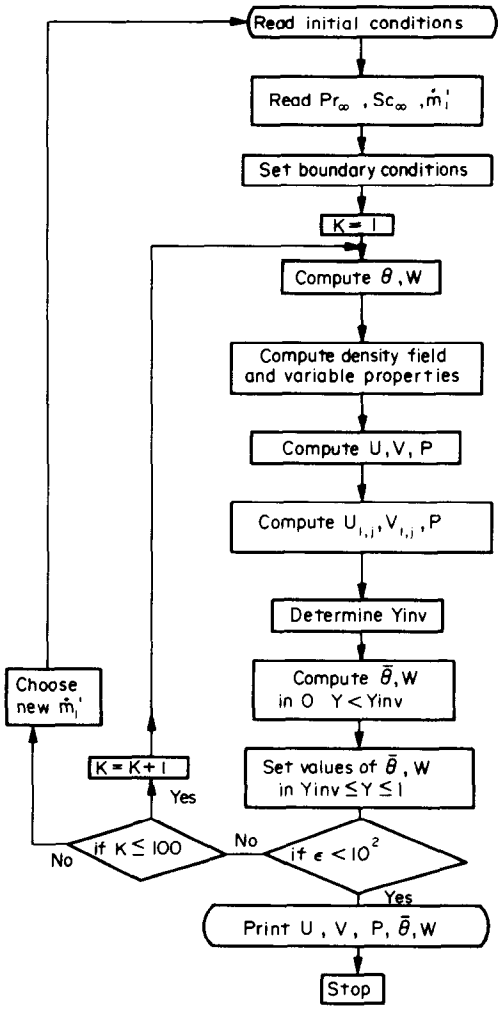

FIG. 2. Flow chart for numerical computations.

The boundary conditions at the inlet ($X = 0$) and exit ($X = 1/Gr_m$) ends of the channel are, of course, time dependent. However, the initial distributions of U, V etc. are known and are the same as $\hat{U}(0, Y)$, $\hat{V}(0, Y)$ etc., and

$$\hat{U}\left(\frac{1}{Gr_m}, Y\right), \quad \hat{V}\left(\frac{1}{Gr_m}, Y\right)$$

etc. At the beginning of each time step, updated values of $U(0, Y)$, $V(0, Y)$ etc. are first computed at the channel inlet and exit to serve as boundary conditions on the low field for that time step.

The boundary conditions at the channel inlet (and exit) for time step $(n + 1)\Delta\tau$ were determined from the knowledge of conditions at all grid points at time $n\Delta\tau$. For this determination, the continuity and momentum equations were applied locally at two rows of grid points at the entrance (or exit). The axial velocity distribution at the entrance (or exit) could thus be determined at time $(n + 1)\Delta\tau$. The location of zero axial velocity point within the entrance (or exit) row of grid points was determined by linear interpolation. The boundary conditions on temperature and concentration fields were then determined in the following manner: over the portion of the entrance (or exit) grid line where the axial velocity was directed out of the channel, the temperature and concentration values were determined by local application of energy and species equations between the last and next-to-last grid lines. On the other hand, over the portion of the entrance (or exit) grid line where the axial velocity was directed into the channel, the temperature and concentration were assumed to have their ambient values, i.e. $\bar{\theta} = 0$, $\bar{m} = 0$. The validity of the latter assumption is somewhat questionable in view of the possibility that some of the fluid leaving the channel could be entrained by the entering ambient air. However, comparison with experiments showed that this assumption was quite reasonable and produced results in agreement with the experiments. The details of the determination of the time dependent boundary conditions at the channel entrance and exit for the time step $(n + 1)\Delta\tau$ may be found in [11]:

An alternating direction implicit (ADI) technique to represent the energy and the species equations (equations 5, 6) in finite difference forms was employed to advance the fields of $\bar{\theta}_{i,j}$ and $\bar{m}_{i,j}$ at interior grid points across a time step $\Delta\tau$. The coefficient velocities were treated as constants over each time step for this equation, and all space derivatives were given centered difference representation. The resulting difference equations are implicit in both X and Y directions and, when applied at each grid point in a column or row, yield tridiagonal systems in the unknown quantities $\bar{\theta}_{i,j}^{(n+1)}$ and $\bar{m}_{i,j}^{(n+1)}$.

Following the computation of $\bar{\theta}_{i,j}$ and $\bar{m}_{i,j}$ at the new time step $(n + 1)\Delta\tau$, the fields of density and transport properties may readily be computed from the equations of state. The velocity field is then

Following the computation of $\bar{\theta}_{i,j}$ and $\bar{m}_{i,j}$ at the new time step $(n+1)\Delta q$, the fields of density and transport properties may readily be computed from the equations of state. The velocity field is then computed from the finite difference representation of the momentum and continuity equations. The procedure for this finite difference representation and resulting equations are presented in [11].

The computations were continued until the calculated values of $\bar{\theta}_{i,j}$ and $\bar{m}_{i,j}$ for all grid points changed no more than 1% from their previous time step value, indicating that a steady state solution had been reached. The flow chart for the computations is shown in Fig. 2.

EXPERIMENTAL APPARATUS AND TECHNIQUE

The objectives of the experimental part of the present study were to set up a reversing buoyancy, free convection flow in a vertical channel with appropriate boundary conditions on temperature and transpiration rate at the walls and to measure the temperature and concentration profiles in the channel.

The technique of Mach–Zehnder interferometry was used in conjunction with traversing thermocouple probe measurements to determine the temperature and CO_2 concentration profiles in the channel.

The channel consisted of two electrically heated plates, one porous and the other solid (Fig. 1). The plates were 15 cm high by 40 cm wide. The porous plate was made of sintered bronze, while the solid plate was aluminum. The temperature of each plate was measured at several locations by thermocouples buried to within 0.25 mm of the front surface. During test runs, the porous plate was maintained approx. 7.5°C above the ambient temperature, T_∞, while the solid plate was maintained approx. 30°C above T_∞, giving the temperature ratio R_t of about 0.25. The uniformity of surface temperature as measured by 20 thermocouples on each of the two surfaces was within 0.5°C.

The channel width and parallelism were precisely controlled by a screw-adjustable mounting arrangement. Care was taken to ensure that the connecting links did not interfere with the interferometer light beam or with the flow at the entrance and exit ends of the channel.

Carbon dioxide was supplied from pressurized cylinders to the porous plate assembly after a flow regulator and a flow meter. The entire test section assembly was enclosed in a large cardboard enclosure to minimize disturbance to the channel flow. The enclosure was open-ended at both top and bottom to allow free entrainment of ambient air.

The traversing thermocouple probe consisted of a 44 cm long, 0.075 mm diameter chromel–constantan wire with a butt-welded junction. The wire was stretched across a pair of hypodermic needles which were supported on a traversing mechanism controlled by a micrometer head. The entire traversing mechanism was supported on a hinged plate to align the wire precisely with the channel walls.

The mach–Zehnder interferometer had 5 cm diameter mirrors and beam splitters and used a filtered mercury vapor lamp as the light source to provide a monochromatic light beam at 5461 Å. The test beam was carefully aligned with the channel walls by use of the method of reflection interference [12]. In ordinary boundary layer work, the reference density point is usually included in the interferograms, so that fringe-shift measurements may be carried out with reference to that point. In a channel flow, however, the reference density point does not exist in a flow picture. The fringe shift at various points must therefore be determined by a comparison of flow and no-flow pictures using a white source to produce identifiable fringes, as explained in [13].

If the fringe-shift profile $S(Y)$ and temperature $T(Y)$ are independently determined at a given axial location, then the concentration profile may be calculated by use of the following formula derived in [11]:

$$\chi(Y) = \left(\frac{n_a^{-1}}{n_{CO_2} - n_a}\right)\frac{1}{\phi(Y)}\left[\frac{S(Y)\lambda}{K_a L \rho_\infty} + 1 - \phi(Y)\right]$$

where the refractive indices n are taken at standard conditions: $p = 760$ mm Hg, $T = 273$ K, and a wavelength of 5461 Å as

$$n_a = 1.0002937; \quad n_{CO_2} = 1.0004505.$$

$\chi(Y)$ is the mole fraction of CO_2. The mass fraction may be calculated from

$$m_{CO_2}(Y) = \frac{\left(\frac{M_{CO_2}}{\hat{M}_a} - 1\right)\chi_{CO_2}(Y)}{1 + \left(\frac{\hat{M}_{CO_2}}{\hat{M}_a} - 1\right)\chi_{CO_2}(Y)}.$$

The experiments were run at two different channel widths: $b = 1.0$ and 1.5 cm and two injection rates corresponding to $V_T = 1.0$ and 2.0.

RESULTS AND DISCUSSION

The accuracy of the solutions of the present time dependent method was first tested by comparison with the "marching method" solution for undirectional flow. For this purpose the CO_2 transpiration rate V_T was set at a vanishing small value so that species buoyancy force was essentially negligible. Comparison was then made between the solutions of the asymmetrically heated walls problem achieved by the two independent methods. For the marching method approach, a finite difference scheme similar to that of [8] was used with the appropriate inlet pressure conditions as suggested by [9]. The results of this comparison are shown in Figs. 3(a, b). It may be seen that the agreement of the non-dimensional temperature and velocity profiles predicted by the two methods is excellent.

The accuracy of the marching method solution was

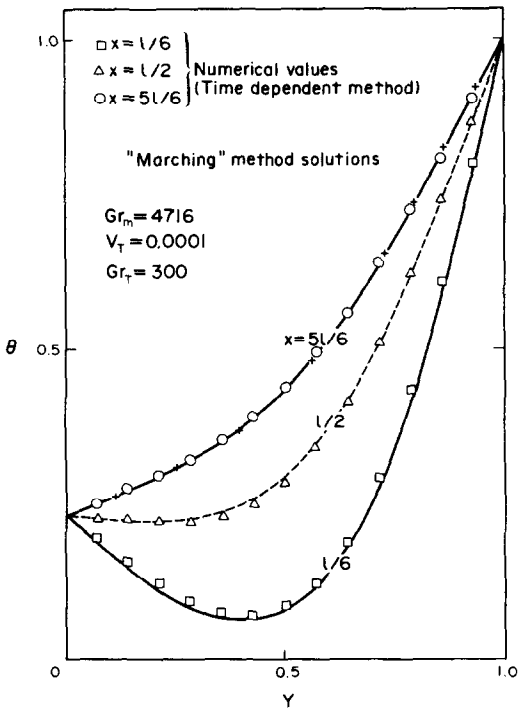

FIG. 3(a). Comparison of temperature profiles calculated by time dependent and marching methods.

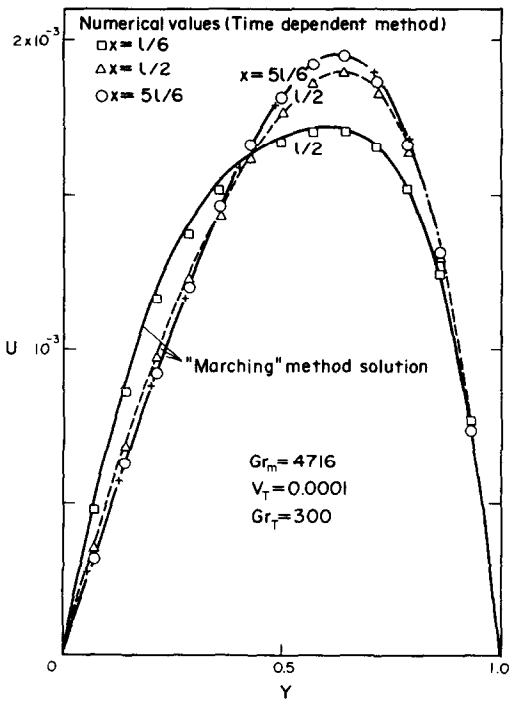

FIG. 3(b). Comparison of velocity profiles calculated by time dependent and marching methods.

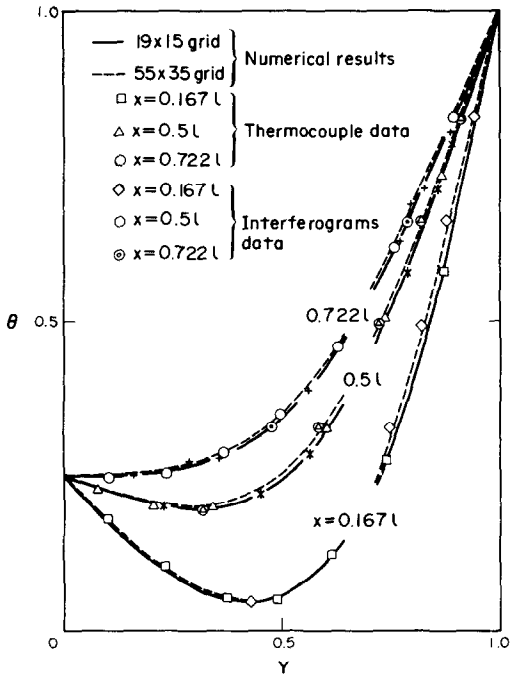

FIG. 4. Comparison of measured and calculated temperature profiles with heated walls and no transpiration.

verified by comparison with the results of two different experimental techniques. The temperature profiles in a channel with heated walls and no CO_2 injection were measured by the traversing thermocouple probe and by inteferometry. This comparison is shown in Fig. 4. It may be seen that marching method solution for this undirectional flow problem predicts data very well. It may also be seen that the differences in prediction between a 19 × 15 grid and a 55 × 35 grid are not too significant.

In order to provide an insight into the nature of a reversing buoyancy flow field in the channel, computations were first carried out at a rather low value of CO_2 injection rate ($V_T = 0.01$), and the effect of increasing wall temperature was investigated. The injection rate employed in this initial computation was much lower than that employed in the experiments.

The streamline plots in Fig. 5 show the effect of progressively increasing the Grashof number Gr_T by increasing the wall temperature, while keeping the CO_2 injection rate fixed at $V_T = 0.01$. At $Gr_T = 50$, most of the flow in the channel is downward, except near the solid wall ($Y = 1$), where the flow is upward. The dashed line shows the locus of points where $u = 0$, and marks the boundary between the regions of upward and downward flow. As Gr_T is increased, the region of downward flow narrows toward the porous wall ($Y = 0$). At still higher Gr_T, a recirculation region develops which is pushed upward as Gr_T is further increased.

The corresponding axial velocity profiles are shown in Fig. 6 for three axial locations in the channel. It may be seen that, when downward flow dominates in the

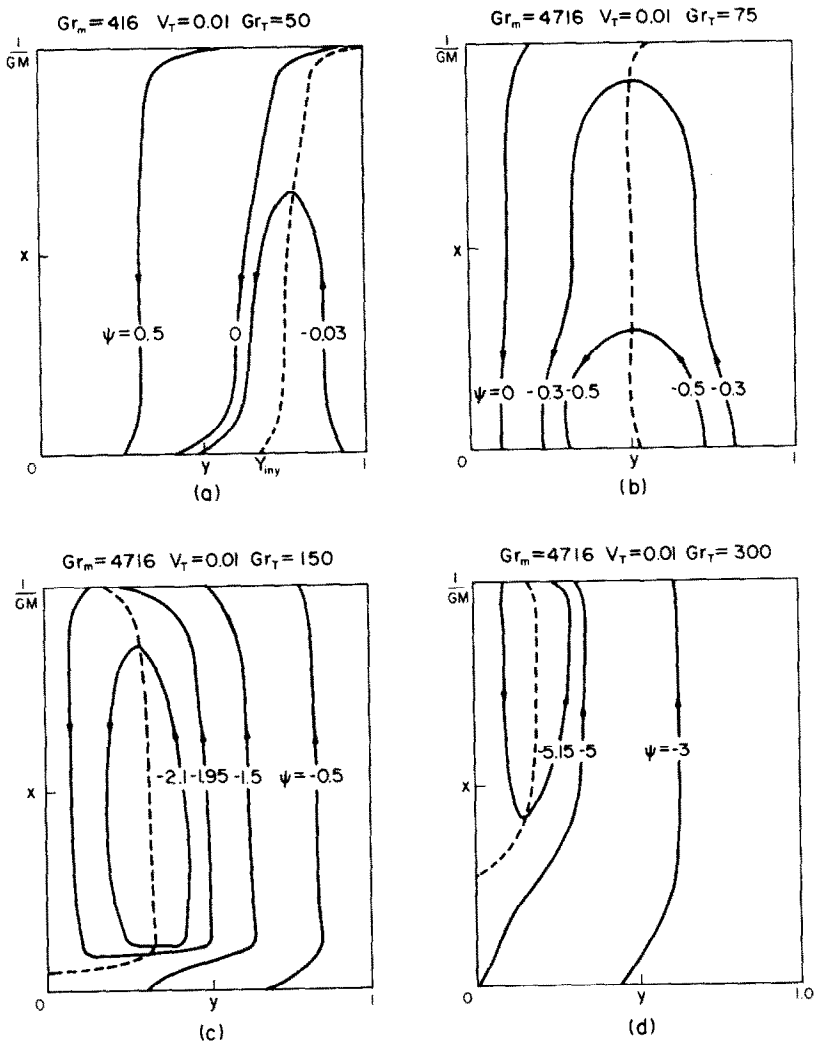

FIG. 5. Calculated streamline plots showing effects of increasing wall temperature at a fixed injection rate.

channel (low Gr_T), the peak velocity decreases in the flow direction for upward flow while increasing in the flow direction for downward flow. On the other hand when upward flow dominates (high Gr_T), the peak velocity increases in the streamwise direction for upward flow and decreases in the flow direction for downward flow.

Results of computations at higher injection rates ($V_T = 0.2$) are shown in Fig. 7 where the velocity profiles at the mid-section ($x/l = 0.5$) are plotted with the parameter Gr_T varying from 0 to 700. For $Gr_T = 0$ (unheated wall) the flow is entirely downward due to the introduction of CO_2 into the channel through the porous wall. As the wall temperatures are progressively increased, the flow close to the solid wall gradually turns upward and the peak upward velocity increases in magnitude with Gr_T.

For a given Grashof number, $Gr_T = 500$, the velocity profiles at three different axial locations are shown in Fig. 8. It is clear that, at this Gr_T value, downward flow still dominates in the channel as the peak upward velocity decreases in the flow direction.

The net mass flow in the upward or downward direction may be determined at different elevations in the channel by integrating these velocity profiles and taking into account the variation of density. In particular, the net upward mass flow at the entrance ($x = 0$) and exit ($x = l$) of the channel was determined. The difference between the two mass flow rates, i.e.

$$\Delta\dot{m}_{x=l} = (\dot{m}_{x=0} - \dot{m}_{x=l})_{\text{upward}}$$

is shown in Fig. 9 as a function of Grashof number Gr_T.

Notice that at low Gr_T (< 100) the flow in the channel is almost entirely downward. Consequently, the upward mass flows at both the entrance and exit are nearly zero. As Gr_T is progressively increased, the upward mass flow entering the channel at $x = 0$ remains larger than that exiting at $x = l$. This shows that some of the upward flowing fluid is entrained by downward flow in the channel. At very large Gr_T, the flow in the channel would be entirely upward and the curve of $\Delta\dot{m}_{x=l}$ would approach an asymptotic limit

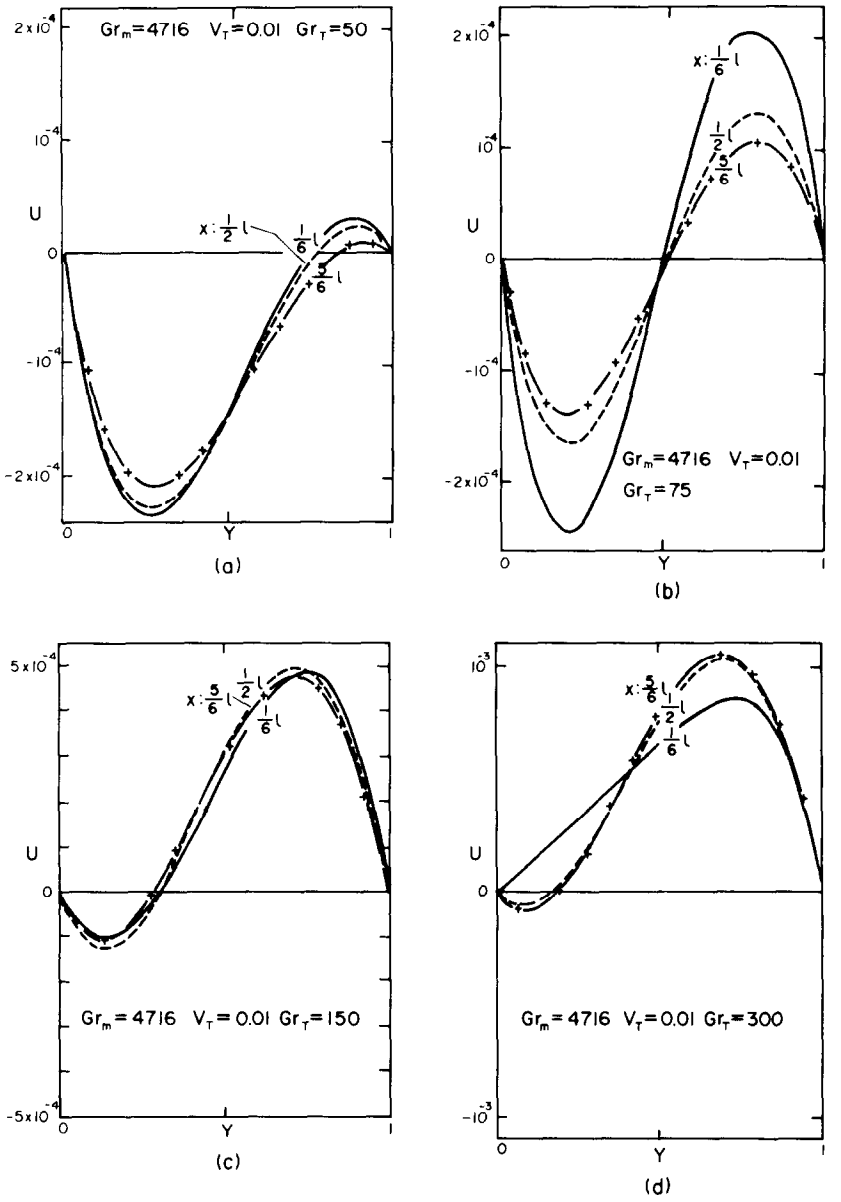

FIG. 6. Calculated velocity profiles in the channel: effect of increasing wall temperature at a fixed injection rate.

of $-(\dot{m}_o'' \cdot l)$ (or -0.67×10^{-4} in non-dimensional coordinates) which is the total mass of fluid introduced into the channel through the porous wall.

A comparison of the present numerical predictions with experiments is shown in Figs. 10 and 11. In Fig. 10, thermocouple-measured temperature profiles at three axial locations for the case $Gr_m = 4716$, $Gr_T = 440$, $R_t = 0.25$ and $V_T = 0.2$ are compared with predictions. The agreement is seen to be excellent. The corresponding concentration profiles are shown in Fig. 11, where the agreement is satisfactory within experimental uncertainty. The corresponding velocity profiles were not measured in the present study. However, Fig. 12 shows the prediction at conditions identical to the ones under which experimental were conducted. Large regions of flow reversals are indeed seen to be present under these conditions.

CONCLUSIONS

A stable, reversing buoyancy, natural convection flow field in a vertical channel was set up successfully in the present experiments. Temperature and concentration profiles in such a flow field were measured by combined use of a traversing thermocouple probe and Mach–Zehnder interferometry. The time dependent method of solution was successfully applied to predict the complex flow field in the channel. The predicted temperature and concentration profiles agree well with measurements.

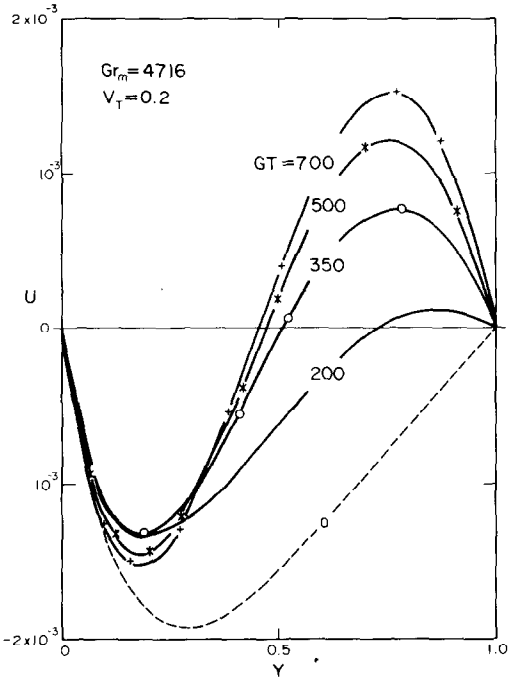

FIG. 7. Calculated velocity profiles in the channel at $x/l = 0.5$: effect of increasing wall temperature at a fixed injection rate.

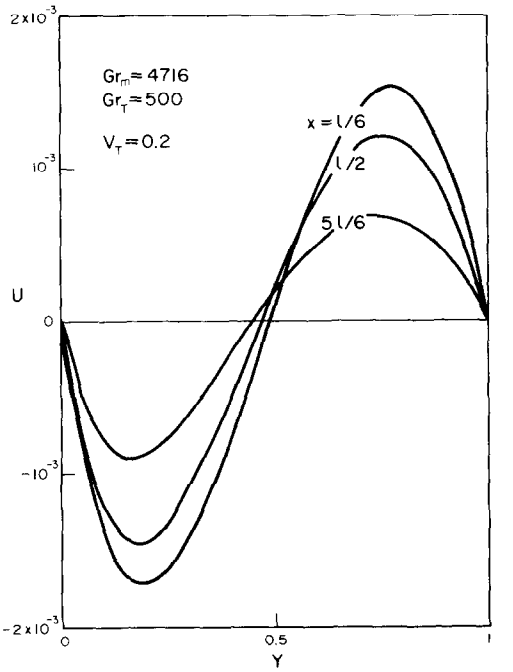

FIG. 8. Calculated velocity profiles in the channel at different elevations.

REFERENCES

1. V. P. Carey, B. Gebhart and J. C. Mollendorf, Buoyancy Force Reversals in Vertical Natural Convection Flows in Cold Water, *J. Fluid Mech.* **97**, 279–297 (1980).
2. M. S. Bendell and B. Gebhart, Heat Transfer and Ice-Melting in Ambient Water Near Its Density Extremum, *Int. J. Heat Mass Transfer* **19**, 1081–1087 (1976).
3. B. Gebhart and L. Pera, The Nature of Vertical Natural Convection Flows Resulting from the Combined Buoyancy Effects of Thermal and Mass Diffusion, *Int. J. Heat Mass Transfer* **14**, 2025–2050 (1971).
4. J. A. Adams and R. L. Lowell, Free Convection Organic Sublimation on a Vertical Semi-Infinite Plate, *Int. J. Heat Mass Transfer* **11**, 1215–1224 (1968).
5. J. B. Klemp and A. Acrivos, A Method for Integrating the Boundary Layer Equations through a Region of Reverse Flow, *J. Fluid Mech.* **53**, 177–191 (1972).
6. J. B. Klemp and A. Acrivos, A Moving-Wall Boundary Layer with Reverse Flow, *J. Fluid Mech.* **76**, 363–381 (1976).
7. P. G. Parikh, Laminar Free Convection on a Vertical Porous Wall with Transpiration and Binary Diffusion. Ph.D. dissertation, Stanford University (1977).
8. J. R. Bodoia and J. F. Osterle, The development of Free Convection between Heated Vertical Plates, *ASME J. Heat Transfer* (Feb. 1962).
9. T. Aihara, Effect of Inlet Boundary Condition on Numerical Solutions of Free Convection between Vertical Paral-

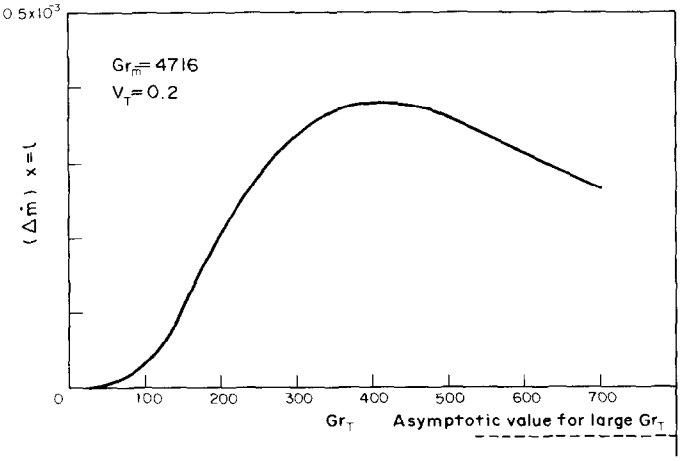

FIG. 9. Differential upward mass flow in the channel.

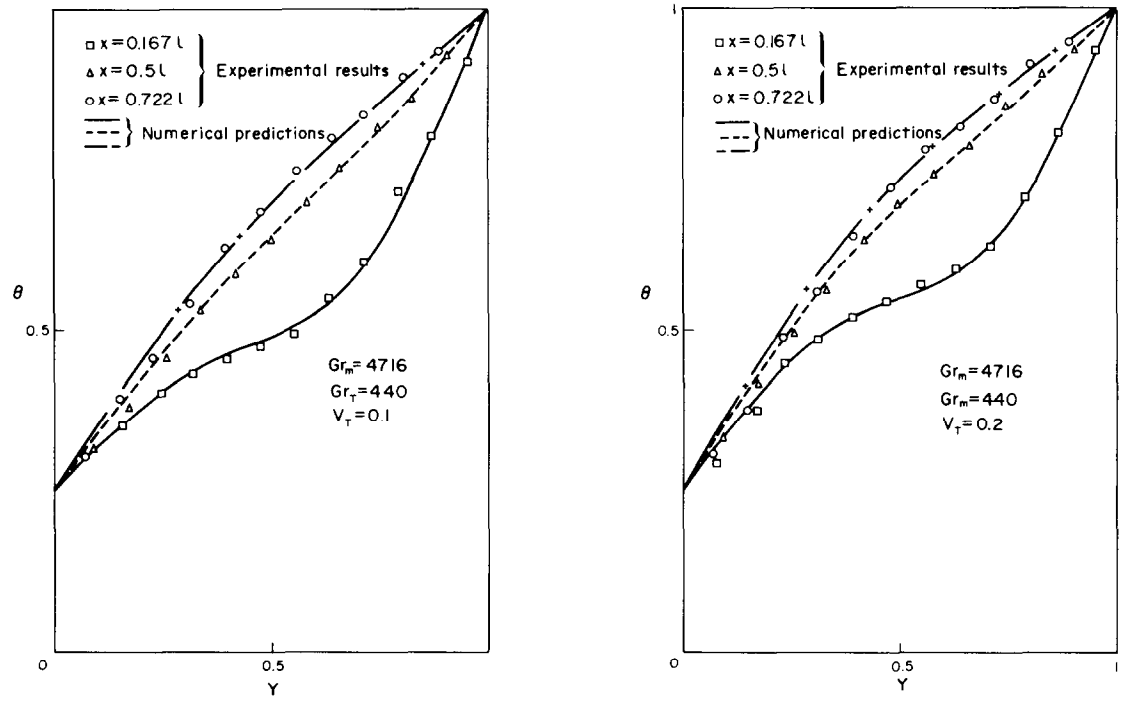

FIG. 10. Comparion of measured and predicted temperature profies.

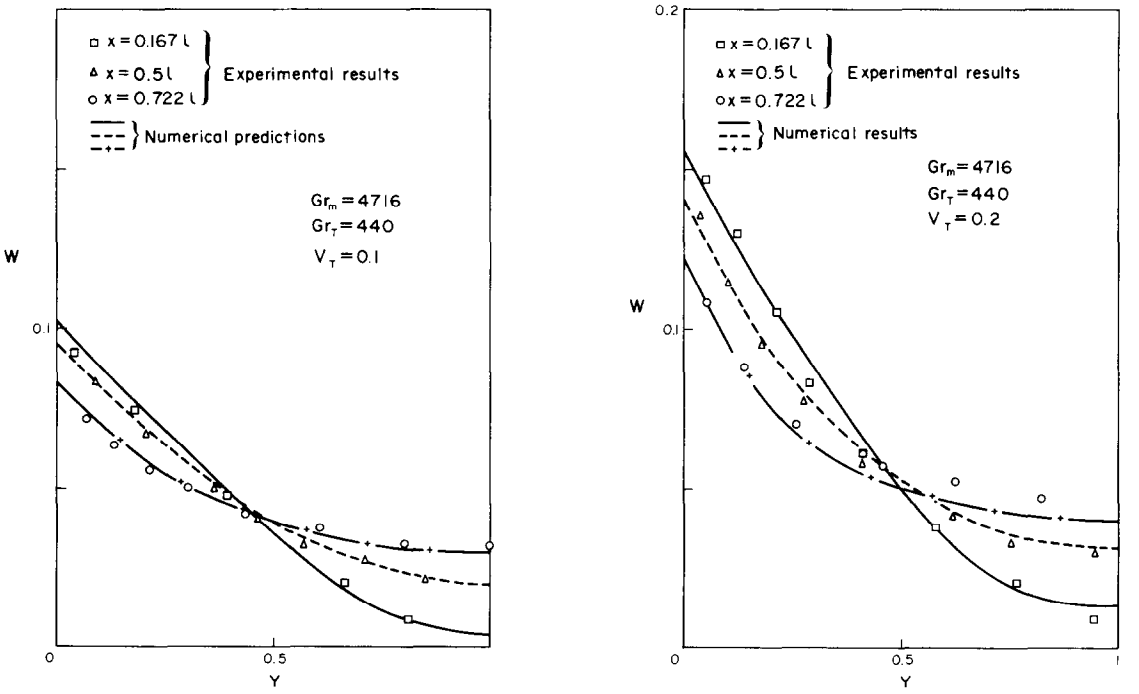

FIG. 11. Comparion of measured and predicted concentration profiles.

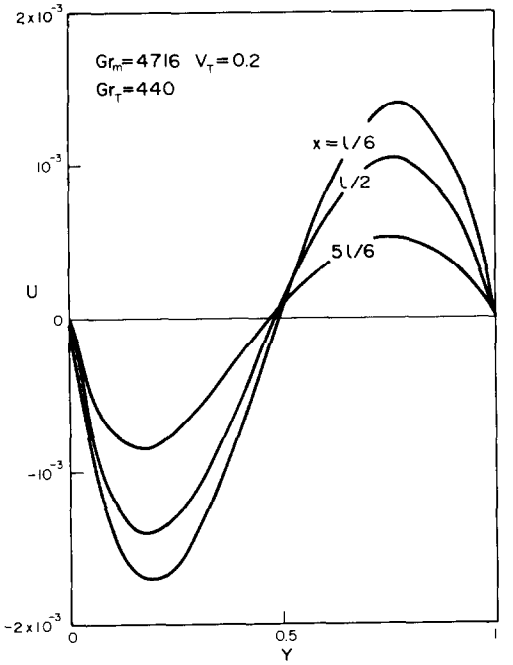

FIG. 12. Predicted velocity profiles under the conditions of experiments.

lel Plates, Report No. 258 of the Institute of High-Speed Mechanics, Tohoku University (1973).
10. J. Quintiere and W. K. Mueller, An Analysis of Laminar Free and Forced Convection between Finite Vertical Parallel Plates, *ASME J. Heat Transfer* **95(c)**, 53–59 (1973).
11. T. S. Lee, Natural Convection in a Vertical Channel with Heat and Mass Transfer and Flow Reversal. Ph.D. dissertation, Stanford University (1979).
12. W. Hauf and U. Grigull, Optical Methods in Heat Transfer, *Advances in Heat Transfer*, Vol. 6, pp. 136–366. Academic Press (1970).
13. R. Ladenburg and D. Bershader, Physical Measurements in Gas Dynamics and Combustion, Vol. IX, pp. 47–75. (Princeton series in *High Speed Aerodynamics and Jet Propulsion*) (1954).
14. W. M. Rohsenow and H. Y. Choi, *Heat Mass, and Momentum Transfer*. Prentice-Hall (1961).

CONVECTION NATURELLE DANS UN CANAL VERTICAL AVEC DES FORCES MASSIQUES EN OPPOSITION

Résumé—La convection naturelle dans un canal vertical, avec des forces massiques qui changent de signe, est étudiée expérimentalement et théoriquement. Le montage expérimental comprend un canal entre deux plaques verticales, l'une poreuse, l'autre pleine. Les deux plaques sont maintenues à des températures uniformes supérieures à celle de l'ambiance et un gaz lourd (CO_2) transpire à travers la plaque poreuse vers le canal. Les champs de température et de concentration de CO_2 sont mesurés en utilisant une sonde à thermocouple et l'interférométrie Mach–Zehnder.

Les champs de température et de concentration sont calculés par une méthode aux différences finies appliquées aux équations de couche limite non stationnaires. Comme les équations sont paraboliques vis-à-vis du temps, la solution peut être cherchée en utilisant des différences finies centrées pour les dérivées spatiales jusqu'à ce que la solution de régime permanent soit atteinte. Un schéma de différences finies peut être construit qui soit stable quelque soit le signe de la composante de vitesse.

Les solutions obtenues montrent plusieurs aspects de cet écoulement complexes en incluant les effets des forces massiques opposées sur les profils de vitesse. Les profils mesurés de température et de concentration montrent un bon accord avec les prévisions théoriques.

FREIE KONVEKTION MIT ENTGEGENWIRKENDEN AUFTRIEBSKRÄFTEN IN EINEM VERTIKALEN KANAL

Zusammenfassung—Die freie Konvektion in einem vertikalen Kanal, in dessen Innerem die Auftriebskraft ihr Vorzeichen ändert, ist experimentell und theoretisch untersucht worden. Der experimentelle Aufbau bestand aus einem von zwei vertikalen Platten begrenzten Kanal, von denen die eine porös und die andere dicht war. Beide Platten wurden auf gleichförmiger Oberflächentemperatur oberhalb der Umgebungstemperatur gehalten, wobei durch die poröse Platte ein schweres Gas (CO_2) in den Kanal eingeführt wurde. Im Kanal wurde durch gleichzeitige Anwendung einer Thermoelementsonde und eines Mach-Zehnder-Interferometers die Temperatur- und CO_2-Konzentrationsverteilung gemessen.

Die Temperatur- und Konzentrationsverteilungen wurden ferner aus einer Lösung der zeitabhängigen Grenzschichtgleichungen mittels endlicher Differenzen bestimmt. Da die zeitabhängigen Gleichungen parabolisch in der Zeit sind, kann die Lösung mit Hilfe zentraler Differenzen für die räumlichen Ableitungen in vorwärtsgerichteten Zeitschritten ermittelt werden, bis eine stationäre Lösung erreicht ist. Somit kann ein Schema mit endlichen Differenzen aufgestellt werden, das unabhängig vom Vorzeichen der Geschwindigkeitskomponente in Strömungsrichtung stabil ist. Die so erhaltenen Lösungen zeigen viele interessante Aspekte dieser komplexen Strömung, einschließlich der Einflüsse entgegenwirkender Auftriebskräfte auf die axialen Geschwindigkeitsprofile. Gemessene Temperatur- und Konzentrationsprofile zeigen gute Übereinstimmung mit den theoretischen Berechnungen.

ЕСТЕСТВЕННАЯ КОНВЕКЦИЯ В ВЕРТИКАЛЬНОМ КАНАЛЕ С ПРОТИВОПОЛОЖНО НАПРАВЛЕННЫМИ АРХИМЕДОВЫМИ СИЛАМИ

Аннотация — Экспериментально и теоретически исследуется естественная конвекция в вертикальном канале, в котором подъемная сила меняет знак на противоположный. Экспериментальная система состоит из канала, образованного двумя вертикальными пластинами: одной пористой, а второй сплошной. Поверхности обеих пластин поддерживаются при постоянной температуре, превышающей температуру окружающей среды. Через пористую пластину в канал подается тяжелый газ CO_2. Поля температур и концентраций CO_2 в канале измеряются одновременно с помощью термопары и интерферометра Маха-Цендера. Кроме того, температурные и концентрационные поля определяются путем решения уравнений нестационарного пограничного слоя конечно-разностным методом, используя центральные разности для аппроксимации пространственных производных. Так как уравнения являются параболическими по времени, стационарное решение можно получить методом установления. Таким образом можно получить устойчивую конечно-разностную схему, не зависящую от знака компонента скорости потока. Полученные решения отличаются целым рядом интересных особенностей, характерных для такого сложного течения, в том числе учетом влияния противоположно направленных архимедовых сил на аксиальные профили скорости. Измеренные профили температуры и концентрации хорошо согласуются с результатами теоретических расчетов.